Desmosomal cell cohesion and epidermal differentiation are modulated by dolichol phosphate mannosyltransferase 1 (DPM1) through SERPINB5-dependent mechanisms

Maitreyi Rathod [1], Henriette Franz [1], Vivien Beyersdorfer [1], Marie-Therès Wanuske [1], Karen Leal Fischer [1], Chiara Stüdle [1], Aude Zimmermann [1], Volker Spindler [1]

[1]Department of Biomedicine, University of Basel, Pestalozzistrasse 20, 4056 Basel

CORRESPONDENCE:

Prof. Dr. Volker Spindler

Department of Biomedicine

University of Basel

Pestalozzistrasse 20, 4056 Basel, Switzerland

volker.spindler@unibas.ch

RUNNING TITLE: DPM1 modulates cell-cell adhesion and epidermal differentiation

KEYWORDS: cell-cell adhesion, desmosomes, DPM1, epidermal differentiation, cytoskeletal organization, SERPINB5, TGF-β signalling

ABSTRACT:

Glycosylation is an essential mediator of cell-cell adhesion and epidermal differentiation. We used CRISPR/Cas9-based gene editing to determine the role of dolichol phosphate mannosyltransferase 1 (DPM1), a key enzyme for N- and O-glycosylation. DPM1 loss resulted in weakening of cell-cell adhesion, impaired localization of the desmosome components desmoplakin and desmoglein 2, and cytoskeletal organization defects in human keratinocytes. In a 3D organotypic human epidermis model, loss of DPM1 resulted in impaired differentiation with abnormally increased cornification, reduced thickness of non-corneal layers, and the formation of intercellular gaps in the epidermis. Using proteomic approaches, SERPINB5 was identified as novel interaction partner of desmoplakin, ameliorating the effects of DPM1 loss on cell-cell adhesion and epidermal differentiation. Further analysis showed that the changes induced by DPM1 and SERPINB5 loss were at least in part dependent on elevated TGF-β signalling. Together, we identify DPM1 through SERPINB5 as a novel regulator of cell-cell adhesion and differentiation.

INTRODUCTION:

Desmosomes are vital mediators of intercellular adhesion and are mechanistically linked to several diseases, such as the blistering skin disease pemphigus, arrhythmogenic cardiomyopathy and different cancers[1-3]. Desmosomes are highly ordered complexes comprising of adhesion molecules and plaque proteins. Desmogleins (DSG) 1-4 and desmocollins (DSC) 1-3 belong to the cadherin family of adhesion molecules, which interact in a calcium-dependent manner[4-7]. While desmosomal cadherins mediate cell-cell contacts by means of their extracellular domains, the intracellular domains interact with the armadillo proteins plakophilin (PKP 1-3) and plakoglobin (PG). These connect to desmoplakin (DSP), which links the entire complex to intermediate filaments of the cytoskeleton, thereby providing mechanical strength to cells and tissues[8]. In addition to intermediate filaments, the actin cytoskeleton also has implications on desmosome assembly in vitro, where actomyosin contractility and the cortical actin network are required for membrane translocation and mobility of desmosomal proteins[9]. Cell-cell adhesion not only provides mechanical strength and tissue integrity, but also influences differentiation processes. A well-coordinated balance of cell-cell adhesion via desmosomes, adherence junctions and tight junctions, as well as differentiation into the cornified layer is important to maintain barrier functions[10]. Alterations in several desmosomal components have led to barrier and differentiation defects, highlighting the importance of these desmosomal cadherins for maintaining tissue integrity and to mediate a proper differentiation process[11-15]. However, the precise underlying mechanisms are only partially understood.

Various post translational modifications (PTMs) seem to play an important role in mediating the subcellular localization of desmosomal proteins, and glycosylation serves as an important PTM in this context. Studies have shown the impact of glycosylation in maintaining tissue homeostasis, protein trafficking, cell signalling, proliferation, differentiation, and cell adhesion[16, 17]. Glycosylation is a complex process of glycan processing and maturation with different end products (mannose rich, complex and hybrid). All glycans are built of some basic units comprising mannose, N-acetylglucosamine, galactose, fucose and sialic acid[18]. The dolichol phosphate mannosyltransferase (DPM) complex is an important mediator in this process as it is responsible for donating mannose residues that feed into all glycosylation pathways[19-21]. Defects in DPM1 lead to congenital glycosylation disorders and seizures[22]. DPM1 expression is increased in several cancers including skin cancer (basal cell carcinoma and squamous cell carcinoma, human protein atlas). With regard to desmosome function, it has been shown that inhibiting N-linked glycosylation results in impaired desmosome formation and stability[23]. It has also been demonstrated that N-linked glycosylation at multiple sites is responsible for the incorporation of DSC2 in the plasma membrane[24]. Further, O-linked glycosylation of PG at N-terminus protects it from proteolytic degradation and enhances cell-cell adhesion[25]. Apart from its role in mediating cell-cell adhesion, glycosylation has also been studied in context of epidermal differentiation. CRISPR/Cas9-based modifications of several glycosylation genes in organotypic models of epidermis led to differentiation defects[26]. Further, glycosylation was implicated in the process of desquamation and shedding of corneocytes from the surface[27]. However, the molecular mechanisms on how glycosylation modulators regulate cell-cell adhesion and subsequent effects on epidermal differentiation are not well understood.

Here we study the contribution of the DPM complex for desmosomal adhesion and epidermal differentiation using keratinocytes and organotypic models of human epidermis.

RESULTS:

DPM1 modulates cell-cell adhesion and differentiation of human epidermis organotypic model

Glycosylation is well established as an important PTM for modulating cell-cell adhesion. We thus sought to understand the role of the DPM group of glycosylation modulators in regulating desmosomal adhesion. We first generated CRISPR/Cas9-mediated knockouts (KO) of DPM1, DPM2 and DPM3 in HaCaT keratinocytes. In line with the occurrence as a complex, loss of DPM2 or DPM3 led to depletion of DPM1 (**Fig S1A**). Dispase-based intercellular adhesion assays showed that loss of DPM1, and to milder extents loss of DPM2 and DPM3, impaired intercellular adhesion, indicated by an increased number of fragments after applying shear stress (**Fig 1A, B**). A KO for the desmosomal protein DSG2 was used as a control for reduced cell-cell adhesion. CRISPR/Cas9-mediated KO of DPM1 in primary human keratinocytes also resulted in loss of cell-cell adhesion, supporting the relevance of DPM1 for keratinocyte intercellular adhesion (**Fig1C, D**). Interestingly, biochemical characterization of desmosomal proteins in HaCaT keratinocytes upon loss of the DPM complex showed no major changes in total protein content (**Fig S1B, C**). Human epidermis is a stratified epithelium that differentiates into several layers on its course of maturation to provide a fully functional epidermis. The basal layer is the layer where keratinocytes proliferate and delaminate, and then differentiate through the spinous, granular and corneal layers (**Fig 1E**). Immunostainings of DPM1 in human foreskin tissue showed expression in all layers of differentiated epidermis, indicating a contribution of this protein in epidermal homeostasis (**Fig S1D**). We generated organotypic 3D-reconstructed human epidermis (3D-RHE) which reproduce the differentiation process of interfollicular epidermis as indicated by CK10 and filaggrin staining and which also showed a similar pattern for DPM1 expression (**Fig S1D, E**). Depletion of DPM1 in 3D-RHEs caused defects in the normal differentiation process, indicated by thickening of the corneal layer and reduced thickness of the other layers, with the total epidermal thickness being unchanged (**Fig 1F-I**). These changes were unrelated to proliferation in the basal layer under DPM1 loss, as indicated by the proliferation marker Ki67 being similar in both sgNT1 and sgDPM1 conditions (**Fig 1J**). Further, DPM1 loss was accompanied by presence of intercellular spaces within the viable layers of the epidermis, indicating perturbed cell-cell adhesion (**Fig 1K**). Biochemical analysis of primary human keratinocytes in 2D cultures transduced with sgNT1 and sgDPM1 showed increased expression of DSC1 and DSG1 upon calcium-induced differentiation, which are desmosomal cadherins that are expressed in later stages of differentiation (**Fig S1F, G**). This supports the notion of altered differentiation by DPM1 loss in 3D-RHEs.

Loss of DPM1 impairs desmoplakin surface localization and cytoskeletal arrangements in human keratinocytes

Based on the biochemical analysis, changes in the protein expression of desmosomal components did not account for the reduced intercellular adhesion upon loss of DPM1. We thus investigated the localization of the essential desmosomal protein desmoplakin (DSP) in HaCaT and primary human keratinocytes. Because DPM1 is the enzymatically active protein of the complex, we focus on DPM1 for further experiments. DSP was significantly reduced at cell borders upon loss of DPM1, indicating reduced number of desmosomes (**Fig 2A, B**). DSG2, which is a desmosomal cadherin specifically clustering in desmosomes[28], was also reduced at the cell membrane under sgDPM1 conditions in HaCaT keratinocytes. DPM1 KO also led to reduced DSP and DSG2 at the cell membrane in primary human keratinocytes, reproducing the findings obtained in HaCaT keratinocytes (**Fig 2C**). Interestingly, DSP appeared fragmented and more cytosolically localized

in the 3D-RHE with sgDPM1 compared to NT1 control (**Fig 2D**). With DSP serving as anchor for keratin intermediate filaments, we also tested whether the reduced DSP membrane localization is associated with changes in keratin distribution in DPM1 KO cells. Pan-cytokeratin staining showed a redistribution away from cell-cell contact sites, creating gaps in the dense keratin network. Further, individual keratin filaments appeared thickened under loss of DPM1 (**Fig 2E, F**). Depletion of DPM1 also led to redistribution of the actin cytoskeleton, where we observed that the cortical actin belt under control conditions was replaced by a more diffuse appearance in the cytosol (**Fig 2G, H**). Changes in the cytoskeletal organisations have effects on the mechanical properties of the cell [29]. Thus, we used an atomic force microscopy (AFM)-based approach to quantify the elasticity of both control and DPM1 KO HaCaT keratinocytes. DPM1 KO cells showed significantly reduced cellular elasticity, quantified as young's modulus (**Fig 2I**). Further, to address whether the reduced expression of DSP on the surface in DPM1 KO conditions correlates with changes in the stability, we performed Fluorescence Recovery After Photobleaching (FRAP) experiments to assess the dynamics of DSP at cell-cell interfaces. FRAP showed a significant increase in the mobile fraction of DSP, indicating altered desmoplakin stability to cell junctions upon loss of DPM1 (**Fig 2J, K**).

Proteome analysis suggest SERPINs as mediators of the changes in adhesion and differentiation upon loss of DPM1

As the DPM complex mediates essential steps of glycosylation, we tested whether loss of DPM1 results in altered glycosylation patterns of DSG2 or DSP. PNGase F-based mobility shift assay showed that DSG2 migrates at a lower molecular weight upon treatment with PNGase F (cleaves all N-linked oligosaccharides) indicating DSG2 is glycosylated. However, we did not observe differences in the migration pattern between sgNT1 and sgDPM1 cells. DSP showed no mobility shift upon PNGase F treatment (**Fig S2A**). This indicates that the altered localization of these molecules is independent of potential N-linked glycosylation. To gain more mechanistic insights into the regulatory roles of DPM1 on desmosomes, we used a global proteomics approach to identify differentially regulated proteins in DPM1 KO HaCaT keratinocytes. Heat map analysis showed distinct sets of genes differentially modulated in both cell types, indicating DPM1 loss has profound changes on the proteome of HaCaT keratinocytes (**Fig S2B, S2C**). Glycoproteins, proteases and regulators of various metabolic pathways, such as carbohydrate metabolism, nitrogen compound metabolic process and purine metabolism pathways were downregulated in DPM1 KO cells. Additionally, several proteins of the SERPIN group were also significantly downregulated in DPM1 KO conditions, while various keratins, RAB GTPase and some Sec complex proteins were upregulated (**Fig 3A**). String-based pathway analysis of differentially expressed proteins showed that the processes of cornification, actin filament assembly, cytoskeletal reorganization and protein folding were significantly upregulated upon loss of DPM1. Upregulation of cornification and cytoskeletal organization pathways might explain enhanced cornification and cytoskeletal changes observed upon loss of DPM1. Vice versa, many metabolic pathways such as purine ribonucleoside, glycosyl compound metabolic pathway, carbohydrate derived metabolic process, catabolic processes, nitrogen metabolic process were downregulated upon loss of DPM1 (**Fig 3B**). In addition to the global changes observed, we were also interested in identifying differential interacting partners of DSP, since we saw major impairments in DSP surface localization and stability. DSP immunoprecipitation-based (**Fig S2D**) targeted mass spectrometry outlined binding partners of DSP enriched in sgNT1 or sgDPM1 cells (**Fig 3C**). Interestingly, SERPINB5 appeared as the most differential hit, with an interaction with DSP being present in control cells only. Overexpression of SERPINB5-GFP in sgNT1 cells and GFP-based pull down of the fusion protein

confirmed interaction with DSP (**Fig 3D**). In line with these observations, we noted a reduced expression of SERPINB5 in DPM1 KO HaCaT keratinocytes by western blot and immunofluorescence-based assays (**Fig S2E-H**). Because global proteome data also showed several proteins of the SERPIN group downregulated in DPM1 KO cells, we were interested in understanding the role of SERPINs in modulating DSP localization and cell-cell adhesion. In addition to SERPINB5, we expressed SERPINB3 and SERPINB4 as GFP fusion constructs in DPM1 KO HaCaT keratinocytes (**Fig S2I**). In dispase-based dissociation assays, both SERPINB3 and SERPINB5 significantly rescued loss of cell-cell adhesion in response to DPM1 loss, while SERPINB4 showed no protective effect (**Fig 3E, F**). Focusing on SERPINB5 we confirmed that expression of SERPINB5 also rescued loss of cell cohesion induced by sgDPM1 in primary human keratinocytes (**Fig S2J**).

SERPINB5 expression rescues desmoplakin localization and cytoskeletal distribution

Overexpression of SERPINB3, SERPINB4 and SERPINB5 in HaCaT keratinocytes showed no major biochemical changes in desmosomal protein expression (**Fig S3A, B**). However, SERPINB5 overexpression in DPM1 KO background led to rescue of DSP localization at cell borders, indicating enhanced number of desmosomes under SERPINB5 rescue. SERPINB4, which showed no protective effect with regard to intercellular adhesion, did not ameliorate DSP membrane localization (**Fig 4A, B**). Similarly, SERPINB5 overexpression in primary human keratinocytes under DPM1 KO condition rescued DSP localization (**Fig 4C**). Consistent with these effects, SERPINB5 overexpression in DPM1 KO cells led to keratin organization similar to controls (**Fig 4D, E**), and a more regular distribution of the cortical actin belt underneath the plasma membrane (**Fig 4F, G**). These changes upon SERPINB5 rescue were also reflected in the mechanical properties of the cells, where SERPINB5 overexpression in HaCaT keratinocytes resulted in an increase in cell elasticity (**Fig 4H**). To address if SERPINB5 modulates DSP without the background of DPM1 loss, we targeted SERPINB5 by CRISPR/Cas9 (sgSERPINB5) in HaCaT keratinocytes (**Fig S3C**). Dissociation assays revealed significant loss of cell-cell adhesion in sgSERPINB5 cells (**Fig 4I, J**). In line with these observations, loss of SERPINB5 led to significantly reduced DSP localization at the cell membrane, indicating reduced desmosome numbers (**Fig 4K, L**). Thus, SERPINB5 modulates DSP membrane localization, even though the total protein levels of DSP remained unaltered (**Fig S3A, B**).

SERPINB5 rescues DPM1 induced differentiation defects in 3D-RHEs

Given the role of SERPINB5 in positively regulating cell-cell adhesion and DSP membrane localization in HaCaT and primary human keratinocytes, we asked if this would be reflected by changes in epidermal differentiation. Primary human keratinocytes transduced with sgDPM1 and either GFP empty or SERPINB5-GFP (**Fig 5A**) were allowed to differentiate for 12 days. Similar to **Fig 1F**, DPM1 KO epidermis expressing GFP showed a thick cornified layer and intercellular gaps were visible, indicating impairments in cell-cell adhesion. Upon SERPINB5 overexpression, the cornified layer was significantly thinner and comparable to the normal control conditions (**Fig 5B, C**). However, the thickness of the viable layers remained unchanged, resulting in a reduced total thickness of epidermis (**Fig 5D, E**). In line with increased intercellular adhesion in response to SERPINB5 expression, the occurrence of intercellular gaps was also significantly diminished in SERPINB5-GFP expressing 3D-RHE (**Fig 5F**). Expression of SERPINB5-GFP in sgDPM1 3D-RHEs also led to enhanced expression of DSP on the cell surfaces in all layers compared to GFP controls (**Fig 5G, H**).

SERPINB5 links TGF-β signalling and loss of cell cohesion in DPM1 KO conditions

It was previously shown that TGF-β signalling negatively modulates cell-cell adhesion and DSP expression in keratinocytes[30]. TGF-β signalling is also known to regulate SERPINB5 expression in mammary epithelial cells [31]. Further, our proteomic (**Fig 3A**) and western blot data (**Fig S4A**) showed significant reduction of CD109 levels in DPM1 KO cells, which is a known negative modulator of TGF-β signalling [32]. SMAD phosphorylation lies downstream of activated TGF-β type 1/2 receptor signalling and is induced in response to BMP/Nodal ligands. Phosphorylated SMAD1/3/5 (pSMAD1/3/5) was increased in DPM1 KO cells compared to NT1 control cells, which was prevented by overexpression of SERPINB5 (**Fig 6A, B).** Phosphorylated SMAD 2/3 (pSMAD2/3), which is activated downstream of TGF-β ligands and type 1 receptors, showed similar trends (**Fig S4A, B**). This suggests that SERPINB5 may serve as a potential negative modulator of TGF-β signalling. Accordingly, pSMAD 1/3/5 levels were higher upon depletion of SERPINB5 in HaCaT cells without interference with DPM1(**Fig 6C, D**), suggesting that SERPINB5 is a negative regulator of TGF-β signalling. Further, to gain insights into the contribution of activated TGF-β signalling on cell-cell adhesion, we inhibited TGF-β receptor 1 activation by GW788388 in DPM1 KO cells for 24 h (**Fig S4C**). GW788388 treatment blocked intercellular adhesion loss mediated by DPM1 KO (**Fig 6E, F**) and restored DSP membrane localization (**Fig 6G-H**). Furthermore, we asked whether the increased activation of TGF-β upon loss of DPM1 is also a putative mechanism during epidermal differentiation and analysed pSMAD1/3/5 expression in 3D-RHE equivalents. Indeed, pSMAD1/3/5 was activated in sgDPM1 3D-RHE (**Fig 6I-J**), suggesting potential association between DPM1, TGF-β signalling and differentiation in human epidermis.

DISCUSSION:

DPM1 and SERPINB5 may serve as link between differentiation and adhesion

The importance of O-linked and N-linked glycosylation in modulating cell-cell adhesion, desmosomes, epidermal differentiation and wound healing has been established in the past[16, 17]. Since all glycosylation pathways are dependent on a basic mannose unit, we here used CRISPR/Cas9-based gene editing system to knockout DPM1, which is an important mannosyl transferase responsible for donating mannose to all important glycosylation steps. CRISPR/Cas9-based gene editing of DPM1 in 3D organotypic model of human epidermis showed impaired stratification and differentiation, with reduced thickness of the viable epidermal layers and abnormally increased corneal layer thickness. Defects in differentiation were accompanied by intercellular gap formation in the epidermis, indicating loss of cell-cell adhesion. Despite a primary function in providing intercellular adhesion, desmosomal proteins are also known to modulate epidermal differentiation and signalling. As examples, loss of DSC1 and DSG4 lead to differentiation defects in interfollicular epidermis[12, 33]. It was also shown that DSG1 regulates epidermal differentiation, which is mechanistically dependent on EGFR and ERK signalling[34]. Ectopic expression of DSG3 in murine epidermis induces cornification defects and trans-epidermal water loss[35] and DSG3 expression in suprabasal layers results in abnormal differentiation and hyperproliferation[36]. Further, the use of ectodomain-deleted DSG3 and inhibiting peptides led to impaired epidermal differentiation and epithelial morphogenesis[37, 38]. These data all support a role of desmosomal adhesion in contributing to correct differentiation of the epidermis. It is possible that the observed defects in differentiation upon depletion of DPM1 at least in part are mediated by impaired membrane localization of desmosomal molecules and resulting reduced adhesion. Thus, the data are consistent with a role of DPM1, via SERPINB5, for epidermal homeostasis on the level of regulating intercellular adhesion. Although DPM1 is a crucial constituent of glycosylation pathways, it is unclear whether the changes we observed are mediated by altered glycosylation. Our data does not support a direct role of impaired glycosylation for membrane trafficking, as we do not see changes in the migratory behaviour of DSG2 or DSP. However, indirect contributions, e.g., by altered glycosylation of other molecules which may be required for the stability and localization of desmosomal molecules, are of course possible. Further analyses will have to clarify the contribution of altered glycosylation in more detail.

Implications of DPM1 on desmoplakin localization and cytoskeletal organization

DPM1 loss led to reduced cell-cell adhesion, loss of DSP and DSG2 at the cell membrane, and altered keratin intermediate filament (IF) organization. A correctly assembled keratin/desmosome network is essential for strong intercellular adhesion. As examples, a DSP mutant with higher binding affinity to keratin filaments strengthened intercellular adhesion[39]. In line with the data shown here, targeting DSG3 by autoantibodies from pemphigus patients induces uncoupling of keratins from the desmosome and loss of intercellular adhesion[40]. It has also been demonstrated that loss of keratins from keratinocytes confer reduced binding forces and cell-cell junction mobility of DSG3[41]. Keratinocytes deficient for all keratins showed increased PKC-mediated phosphorylation of DSP, leading to destabilization of desmosomes[42]. Further, it has been studied in hepatocytes that keratin 8 loss leads to perturbed DSP expression at the cell membrane[43] and depletion of wound healing keratins K6/17 result in less stable desmosomes[44]. The actin cytoskeleton also appears to be crucial for desmosome assembly. It has been demonstrated that DSP assembly into desmosomes occurs in three stages with the last stage being actin-dependent [9]. Further, the actin binding protein adducin and the cortical actin network are required for DSG3

membrane incorporation and cell-cell adhesion [45, 46]. Vice versa, it has also been shown that desmosomal proteins in turn regulate actin organization in the cells[47, 48]. Interestingly, it was observed that upon loss of type 2 keratins, cortical actin was also reduced, demonstrating an interdependency of cortical actin and IF organization [42]. Interestingly, we found profoundly perturbed keratin and cortical actin organizations in DPM1 KO cells indicating that DPM1 modulates the complex interplay between the different components of the cytoskeleton and adhesion molecules. It is unclear in this context, whether reduced DSP at the cell surface leads to cytoskeletal remodelling or vice versa unstable DSP at cell junctions is a consequence of cytoskeletal impairments. Nevertheless, IF and cortical actin are associated with physical properties of a cell[29] and we observed reduced cellular elasticity in DPM1 KO cells, supporting the altered cytoskeleton defects observed in these cells.

Proteomic analysis of DPM1 KO keratinocytes revealed major alterations in important biological pathways. Interestingly, cornification and cytoskeleton reorganization pathways were significantly upregulated, which are in line with the observed results discussed above. On the other hand, metabolic pathways including carbohydrate metabolism and purine metabolism pathways were significantly downregulated under the loss of DPM1. Indeed, altered metabolic pathways have been directly associated with impaired epidermal differentiation. For example, altered lipid contents in cornified layer is associated with skin conditions, like ichthyosis[49, 50]. Detailed lipidomic analysis revealed specific lipid subsets which regulated epidermal differentiation and helped keratinocytes exit from the stem cell compartment[51]. Glucose metabolism is also important in maintaining skin homeostasis. mTOR pathway regulates glycolysis and mTOR effectors Rheb and Raptor KO in mice leads to differentiation defects in epidermis and reduced desmosomes[30]. In light of these data it may be speculated that DPM1-mediated defects in epidermal differentiation are dependent on altered metabolic pathways, however this requires further investigation.

SERPINB5 mediates desmoplakin localization and intercellular adhesion

In an attempt to dissect the mechanisms underlying altered cell-cell adhesion in keratinocytes, we immunoprecipitated DSP, which was subjected to proteomic analysis. While SERPINB5 showed interaction with DSP in control cells, the interaction was not detected in DPM1 KO cells. This drew our attention to SERPINs as we observed downregulation of several SERPIN family members in DPM1 KO cells. The SERPIN class of proteins are classical serine peptidase inhibitors, however, SERPINB5 (MASPIN) is an exception. SERPINB5 does not have peptidase inhibitor activity[52] and was studied majorly in breast cancer where it modulates cell adhesion, migration and apoptosis of tumour cells[53-56]. SERPINB5 was shown to be regulated by EGFR and through cell density[57], however how SERPINB5 modulates cell-cell adhesion and epidermal differentiation was not clear. BioID screening of DSP interactors have shown the existence of SERPINB5 in the inner dense plaque of the desmosome, supporting our findings[58]. We here confirmed that SERPINB5 is downregulated in DPM1 KO cells and overexpressing SERPINB5 in DPM1 KO cells rescues DSP membrane localization, prevents retraction of keratins and cortical actin alterations. CRISPR/Cas9-based gene editing of SERPINB5 from HaCaT WT keratinocytes showed impaired DSP expression on the cell surface and loss of cell-cell adhesion, confirming that SERPINB5 is a novel regulator of DSP in cultured keratinocytes, however a clear understanding of the precise mechanisms how SERPINB5 regulates DSP is still missing.

TGF-β signalling and SERPINB5 contribute to keratinocyte adhesion and differentiation

DPM1 KO keratinocytes exhibited downregulation of the glycoprotein CD109, which is a known negative modulator of TGF-β signalling pathway[32]. TGF-β signalling was also shown to reduce

cell-cell adhesion and impair DSP expression[30]. In agreement with these data, we saw activation of SMAD1/3/5 and SMAD2/3 in DPM1 KO cells, suggesting that loss of DSP localization was a consequence of TGF-β signalling. Inhibition of TGF-β activation in DPM1 KO cells ameliorated loss of cell-cell adhesion and rescued DSP positioning at the cell membrane. We also observed enhanced activation of SMAD2/3 in organotypic skin models lacking DPM1, indicating altered TGF-β signalling as a putative mechanism of perturbed differentiation in DPM1 KO 3D-RHE. In line with our findings, it has been shown that hyperactive TGF-β signalling in mice leads to thinner epidermis and neonatal lethality[59]. Interestingly, rescuing SERPINB5 in DPM1 KO cells reduced SMAD activity to the level of NT controls. Because we also observed elevated pSMAD1/3/5 levels in SERPINB5 knockout cells, this indicates a negative modulation of TGF-β signalling by SERPINB5. Further, SERPINB5-GFP expression in DPM1 KO 3D-RHEs reduced intercellular gap formation, supporting our notion of rescued cell-cell adhesion. Corneal layer thickening in response to DPM1 loss was also ameliorated by ectopic expression of SERPINB5 in 3D-RHE, although the thinning of the non-corneal epidermis was not affected. Still, this demonstrates an important contribution of SERPINB5 to the DPM1-dependent modulation of cornification. Along similar lines, SERPINB7 was recently shown to modulate epidermal differentiation and loss of SERPINB7 in mice led to psoriasiform lesions [60]. These roles of the SERPINB family members in epidermal differentiation may warrant a more detailed analysis also with regard to conditions such as wound healing.

Taken together, we here showed that DPM1 by modulating SERPINB5 levels contributes to intercellular adhesion and epidermal differentiation. Specifically, DPM1 and SERPINB5 influence DSP membrane localization and the organization of both the keratin and cortical actin network. Finally, in this context, we identified a functional association of SERPINB5 and TGF-β signalling, in which SERPINB5 suppresses the activation of canonical TGF-β pathways and the resulting loss of intercellular adhesion.

FIGURE LEGENDS:

Figure 1: A-B) Dispase-based dissociation assays to semi quantitatively assess cell-cell adhesion in HaCaT keratinocytes (N=4). One-way ANOVA, Dunn's multiple comparison test used for statistics. Higher fragmentation represents lower adhesive strength. **C-D)** Dispase-based dissociation assays of primary human keratinocytes (N=5). Unpaired Student's t-test. **E)** Schematic of epidermis (top) and of 3D-RHE model design from primary human keratinocytes (bottom). **F)** H&E staining and immunostainings for CK10/Filaggrin, DPM1, and Ki67 of control (sgNT1) and DPM1 knockdown (sgDPM1) 3D-RHEs 12 days post airlift. Insets and arrows denote interfollicular gaps in different layers of epidermal equivalents. White dashed line indicates membrane insert. Scale bar indicates 20µm distance. **G-I)** Quantification of epidermal thickness parameters from 6 independent biological replicates, from 2 different donors. Each dot represents one biological replicate. Unpaired Student's t-test. **J)** Analysis showing Ki67-positive nuclei normalised to total number of nuclei (N=3). Unpaired Student's t-test. **K)** Violin plot showing quantification of intercellular spaces within the epidermis in sgNT1 and sgDPM1 3D-RHE. The area for defining intercellular spaces was set to be greater than 50µm^2 to exclude shrinking artefacts. The respective areas were then normalized to the total length of the tissue (µm) region used for analysis. A minimum of 20 individual fields of view were used for analysis from 3 independent biological replicates. Unpaired Student's t-test used for statistical analysis.

Figure 2: A) Immunostaining of desmoplakin (DSP) and desmoglein 2 (DSG2) in HaCaT keratinocytes. Merge indicates overlap between DSP, DSG2 and nuclei stained with DAPI. Scale bar indicates 10µm distance. **B)** Quantification of the number of DSP puncta over the respective length of cell membrane (µm) from individual cells (represented by individual dots), N=3. Unpaired Student's t-test used for statistical analysis. **C)** Immunostaining of DSP and DSG2 in primary human keratinocytes. Scale bar indicates 10µm distance. Panel shows representatives of 3 biological replicates. **D)** Immunostaining of DSP in 3D-RHE of control (sgNT1) and sgDPM1 conditions. White dashed line indicates membrane insert. Magenta dashed rectangles mark regions magnified on the right. Representative of 3 biological replicates. **E-F)** Keratin staining depicted by pan-cytokeratin in control and DPM1 KO HaCaT keratinocytes. Analysis done by quantifying the keratin staining intensity (A.U., Y-axis) across cell borders spanning a defined distance (X-axis). Scale bar indicates 10 µm distance. 30 individual cells were quantified from 3 independent biological replicates. **G-H)** F- actin stained by phalloidin in control and DPM1 KO HaCaT keratinocytes. Analysis done by quantifying the F-actin staining intensity (A.U., Y-axis) across cell borders spanning a defined distance (X-axis). Scale bar indicates 10 µm distance. 30 individual cells were analysed from 3 independent biological replicates. **I)** Depiction of atomic force microscopy setup to measure cellular elasticity. Graph shows cellular elasticity, indicated by young's modulus (kPa). Each dot represents single cells from 3 biological replicates. Unpaired Student's t-test. **J-K)** Kymographs and mobile fraction analysis derived from fluorescence-based recovery after photobleaching (FRAP) assays used to measure DSP stability at cell-cell contact sites (N=3). Each dot represents one biological replicate. Significance calculated by unpaired Student's t-test.

Figure 3: A) Volcano plot showing differential protein expression in sgDPM1 with respect to control sgNT1 HaCaT keratinocytes from 3 biological replicates. -Log 10 p values above 1.3 were considered significant (marked by grey line on plot). Orange dots indicate proteins which were

significantly downregulated in DPM1 KO cells, whereas blue dots indicate proteins that were significantly upregulated in DPM1 KO cells. **B)** String-based biological pathway analysis of significantly modulated proteins (orange: downregulated pathways and blue: upregulated pathways). X-axis denotes false discovery rate (FDR), with a cutoff set to 0.05 for significance. **C)** Heat map showing differential binding partners of DSP in sgNT1 and sgDPM1 cells (N=3). Colour codes represent differential mean intensity values, arbitrary unit (A.U.) **D)** Co-immunoprecipitation assay showing DSP binding to SERPINB5 (expressed as SERPINB5-GFP in HaCaT sgNT1 cells). GFP served as negative control. **E-F)** Dispase-based dissociation assays with sgDPM1 HaCaT keratinocytes overexpressing SERPINB3, SERPINB4 and SERPINB5. ns indicates non-significant (N=3). Each dot represents one biological replicate. One-way ANOVA, Dunnett's multiple comparision test used for statistical analysis.

Figure 4: A) Images of DSP immunostainings in sgDPM1 and respective SERPIN overexpressing HaCaT keratinocytes. Panel shows representative of 3 biological replicates. Scale bar indicates 10µm distance. **B)** Quantification of the number of DSP puncta on the cell membrane normalised to the length of plasma membrane (µm). Each dot represents individual cells analysed from 3 independent biological replicates. ns indicates non-significant. One-way ANOVA, Dunnett's multiple comparision test used for statistical analysis. **C)** Immunostaining showing DSP localization at the cell membrane upon SERPINB5 overexpression in DPM1 KO primary human keratinocytes. Panel shows representative of 3 biological replicates. Scale bar indicates 10µm distance. **D-E)** Keratin staining depicted by pan-cytokeratin in sgNT1, DPM1 KO and DPM1 KO overexpressing SERPINB5-GFP construct in HaCaT keratinocytes. Analysis done by measuring the keratin intensity at cell junctions (A.U., Y-axis) under a defined distance (X-axis). Scale bar indicates 10 µm distance. 30 individual cells were quantified from 3 independent biological replicates. **F-G)** F-actin staining depicted by phalloidin in sgNT1, DPM1 KO and DPM1 KO overexpressing SERPINB5-GFP HaCaT keratinocytes. Scale bar indicates 10 µm distance. Analysis done by measuring the phalloidin intensity at cell junctions (A.U., Y-axis), under a defined distance (X-axis). 30 individual cells were quantified from 3 independent biological replicates. **H)** Depiction of atomic force microscopy setup to measure cellular elasticity. Graph shows cellular elasticity, indicated by young's modulus (kPa). Each dot represents single cells from 3 biological replicates. Unpaired Student's t-test. **I-J)** Dispase-based intercellular adhesion assays showing reduced cell-cell adhesion upon knockdown of SERPINB5 in HaCaT keratinocytes (N=4). Unpaired Student's t-test used to determine statistical significance. **K-L)** Images and analysis of DSP at the cell membrane upon loss of SERPINB5 (N=3). Each dot represents single cells from 3 biological replicates. Scale bar indicates 10 µm distance. Unpaired Student's t-test used to determine statistical significance.

Figure 5: A) Western blot showing the GFP fused SERPINB5 (molecular weight around 70kDa) expression in primary human keratinocytes that lack DPM1. GFP served as control. GAPDH used as internal loading control. **B)** H&E staining of 3D-RHE from sgDPM1 expressing GFP empty control or SERPINB5-GFP 12 days post airlift. Insets indicate intercellular gaps in the epidermis equivalents. Immunostainings for CK10 and filaggrin used as differentiation markers. Scale bar indicates 20µm distance. White dashed line indicates membrane insert. Panel shows representatives from 3 biological replicates. **C-E)** Quantification of corneal layer thickness, total epidermal thickness and viable (non-corneal) epidermal layer thickness from 3 independent biological

replicates. Statistics tested by Student's t-test, unpaired. **F)** Violin plot showing quantification of intercellular spaces within the epidermis in sgDPM1 GFP empty and sgDPM1 SERPINB5 GFP 3D-RHE. The area for defining intercellular spaces was set to be greater than 50µm^2 to exclude shrinking artefacts. The respective areas were then normalized to the total length of the tissue region (µm), used for analysis. A minimum of 15 individual fields of view were used for analysis from 3 independent biological replicates. Unpaired Student's t-test used for statistics. **G-H)** Immunostaining and analysis of DSP intensity (cyan) in 3D-RHE of sgDPM1 GFP empty and sgDPM1 SERPINB5-GFP conditions. Panel shows representative of 4 biological replicates. Scale bar indicates 20µm distance. Unpaired Student's t-test used to determine statistical significance (N=4).

Figure 6: A-B) Western blot images and representative quantifications of phosphorylated SMAD1/3/5 (pSMAD1/3/5) in HaCaT keratinocytes. GAPDH used as a loading control. Statistical analysis done by One-way ANOVA, Dunnett's multiple comparision test (N=4). Each dot represents individual biological replicates. **C-D)** Western blot showing pSMAD1/3/5 levels in sgNT1 and sgSERPINB5 HaCaT keratinocytes. GAPDH used as loading control. N=4, statistical analysis done by unpaired Student's t-test. Each dot represents individual biological replicates. **E-F)** Dispase-based dissociation assays in sgDPM1 HaCaT keratinocytes upon inhibition of TGF-β type 1 receptor mediated signalling (GW788388 used as an inhibitor of TGF-β receptor activation). DMSO used as vehicle control. Statistical analysis done by unpaired Student's t-test (N=4). Each dot represents individual biological replicates. **G-H)** Images and analysis of DSP expression at the cell membrane. Each dot represents individual cells from 3 biological replicates. Scale bar indicates 10 µm distance. DMSO used as vehicle control. Statistical analysis done by unpaired Student's t-test. **I-J)** Images and analysis showing pSMAD1/3/5 levels in sgDPM1 3D-RHE. DAPI used to stain nuclei. White dashed line indicates membrane insert. Scale bar indicates 20µm distance. Each dot represents individual biological replicates Statistical analysis done by unpaired Student's t-test (N=3).

MATERIALS AND METHODS:

Cell culture and cloning

HaCaT keratinocytes[61] were cultivated at 5% CO2 and 37°C in Dulbecco's Modified Eagle Medium (DMEM) (Sigma-Aldrich, St. Louis, MO, USA) containing 1.8 mM calcium and complemented with 10% fetal bovine serum (Merck, Darmstadt, Germany), 50 U/ml penicillin, 50 µg/ml streptomycin (both AppliChem, Darmstadt, Germany) and 4 mM L-glutamine (Sigma-Aldrich). Primary human keratinocytes were cultured in EpiLife medium (#11684842 Fisher Scientific) containing 0.06 mM CaCl2 (Gibco, Carlsbad, California), supplemented with 1% Human Keratinocyte Growth Supplement (HKGS, #10761364 Fisher Scientific) and 1% Pen/Strep.

For cloning, oligos of sgDPM1, sgDPM2, sgDPM3 and sgSERPINB5 were synthesized by microsynth (sequences mentioned in supplementary table 1), phosphorylated using T4 PNK enzyme (#0201S NEB, Ipswich, MA USA), annealed and ligated into Esp3I-digested (#R0734L NEB) lentiCRISPR_v2 (#52961 Addgene Watertown, USA) vector, using T4 ligase (#M0202S NEB). Ligated product was transformed in competent DH5alpha E. coli strain and plated on ampicillin-containing (100 ug/ml) agar plates. Colonies were amplified in 3 ml medium containing ampicillin (100 ug/ml). Plasmids were isolated via miniprep (#300287 Machery Nagel, Germany) and sequenced with U6_forward primer (GAGGGCCTATTTCCCATGATT).

For cloning SERPINB3, SERPINB4 and SERPINB5 overexpression constructs, PCR of HaCaT cDNA was performed using Platinum SuperFi 2 DNA Polymerase (#16410771 Fisher Scientific) according to manufacturer's protocol and primers listed in table 1. The annealing temperature for the primers was set to 56°C. The PCR product was purified with PCR and gel purification kit (# 28506 Qiagen, Maryland, USA). The PCR product and the plasmid pLenti-C-mGFP (# PS100071 OriGene Technologies, Rockville, MD, USA) were digested with Asc1 (#R0558L Bioconcept, Allschwil, Switzerland) and Xho1 (#300366 NEB) for 3h at 37°C. The digested product was loaded on a 1% agarose gel and purified from the gel with PCR and gel purification kit (# 28506 Qiagen). The insert was ligated into the vector with a ratio of 3:1 overnight at 16°C using T4 Ligase (# 300361 Bioconcept). Positive clones were sequenced with forward and reverse primers (for TAATACGACTCACTATAGGG; rev CTTGATCTCCAGCTTGCCGT for SERPINB4; TCAGTGAAGCCAACACCAAGT for SERPINB3 and GAAAAGGAGCCACTGGGCAA for SERPINB5.

Generation of lentiviral constructs and stable cell lines

Lentiviral particles were generated according to standard procedures. HEK293T cells (between passage 9-11) were transfected with lentiviral packaging vector psPAX2 (#12259, Addgene, Watertown, MA, USA), the envelope vector pMD2.G (#12260, Addgene) and the respective construct plasmid using TurboFect (Thermo Fisher Scientific, Waltham, MA, USA). 48 h post transfection, virus-containing supernatant was collected and concentrated using Lenti-Concentrator (OriGene), for minimum 2 h at 4-degree celsius. Cells were transduced with the respective virus particles in an equal ratio using 5 µg/mL polybrene (Sigma-Aldrich) according to the manufacturer's instructions. 24 h post transduction for HaCaT keratinocytes and 8 h later for primary human keratinocytes medium was exchanged and puromycin selection was given. Cells were cultivated for at least one week under selection, before starting with the respective experiments. Expression of the respective construct was confirmed via western blot analysis.

Isolation of primary human keratinocytes

Foreskin tissue was obtained during circumcision of patients after informed consent according to the local ethical committee (EKNZ; date of approval: 11.06.2018, Project-ID: 2018-00963). Skin samples were washed three times in PBS containing 300 U/mL penicillin (#A1837 AppliChem), 300 U/mL streptomycin sulphate (#A1852 AppliChem) and 7.5 µg/mL amphotericin B (#A2942 Sigma-Aldrich). Excess tissue, blood vessels and parts of the dermis were removed and skin was cut into pieces of 0.5 x 1 cm size. To separate dermis and epidermis, skin samples were digested at 4°C overnight in 5 mg/mL dispase II solution (#D4693 Sigma-Aldrich) in HBSS (#H8264 Sigma-Aldrich) containing 300 U/mL penicillin, 300 U/mL streptomycin sulphate and 2.5 µg/mL amphotericin B. Epidermis was peeled off and washed once in PBS and digested in 0.25% trypsin and 1 mmol/L EDTA containing 100 U/mL penicillin and 100 U/mL streptomycin sulphate at 37°C for 20 min. Trypsin activity was stopped by diluting 1:1 with a 1 mg/mL solution of soy bean trypsin inhibitor (#10684033 Gibco) in PBS. Keratinocytes were isolated by scratching the epidermis fragments on the dish bottom and through a 70 µm cell strainer (#431751 Corning, Somerville, USA). The isolated normal human epidermal keratinocytes (NHEK) were then seeded at a density of ~8×10^4 cells/cm^2 in EpiLife medium containing 60 µmol/L $CaCl_2$ (#MEPI500CA Gibco) and 1% Human Keratinocyte Growth Supplement (#S0015 Gibco), 1% Pen/Strep and 2.5 µg/mL amphotericin B. After 3 days, the medium was exchanged, and from there on amphotericin B was omitted. For experiments, 40,000 cells were seeded in a 24-well plate and grown until they reached confluency. Subsequently, differentiation was induced by adding 1.2 mmol/L $CaCl_2$ for 24 h.

3D Reconstructed Human Epidermis (3D-RHE)

3D-RHE generation was performed according to the provided protocol of CellnTec (CellnTec, Bern, Switzerland). In brief, NHEK cells were cultivated in CnT-PR medium (#CNT-PR CellnTec) to ~50-70% confluency and transduced with respective constructs, as described above. Cells were selected in puromycin (Fisher Scientific) (2µg/ml). The cells were then seeded (1.7 x 10^5 cells per insert) on 0.4 µm polycarbonate 24-well inserts (#10387523 Thermo Scientific) which were coated with 15 µg/cm^2 rat-tail collagen I (#50201-IBIDI, Gräfelfing, Germany) in 0.02 M acetic acid at 37°C for 1 h. NHEKs were cultivated in CnT-PR medium. 24 h after seeding, the medium inside the insert and 6-well was exchanged with CnT-PR-3D medium (#CnT-PR-3D CellnTec). After 16-18 h, inserts were lifted to an air-liquid interface by aspirating the media inside the insert and adding CnT-PR-3D in the 6-well up to the level of the insert membrane (1.3 mL); the CnT-PR-3D medium was exchanged every other day. The 3D organotypic cultures were harvested and analyzed 12 days post-airlifting by fixing in 2% paraformaldehyde at 4°C for 4 h.

Western Blot

Confluent cell monolayers were lysed with SDS lysis buffer (25 mM HEPES, 2 mM EDTA, 25 mM NaF, 1% SDS, pH 7.6) supplemented with an equal volume of a protease inhibitor cocktail (cOmplete, Roche Diagnostics, Mannheim, Germany), by using a cell scraper. Lysates were sonicated and the total protein amount was determined with a BCA protein assay kit (Thermo Fisher Scientific) according to the manufacturer's instructions. The proteins were denatured by heating in Laemmli buffer, for 10 min at 95°C. Membranes were blocked in odyssey blocking buffer (Li-Cor, Lincoln, NE, USA) for 1 h at room temperature. The following primary antibodies

were diluted with odyssey blocking buffer in tris-buffered-saline containing 0.1% Tween20 (TBS-T) (Thermo Fisher Scientific) and incubated overnight at 4°C, with rotation: mouse Dsc2 mAb (#60239-1-Ig Proteintech, Rosemont, IL, USA), mouse Dsg2 mAb (clone 10G11, #BM5016 Acris, Herford, Germany), rabbit Dsg3 pAb (EAP3816 Elabscience, Biozol, Eching, Germany), mouse Pkp1 mAb (clone 10B2, #sc-33636 Santa Cruz, Dallas, TX, USA), mouse Pkp2 mAb (#651101 Progen, Heidelberg, Germany), mouse PG mAb (clone PG5.1, #61005 Progen), mouse DSP mAb (#sc-390975 Santa Cruz), mouse E-Cad mAb (clone 36, #610181 BD Biosciences, Franklin lakes, NJ, USA), rabbit DSC1 mAb (#ab150382 Abcam, Cambridge, UK), mouse DSG1 ((#651111 Progen), rabbit keratin 10 (#905403 Biolegend), mouse keratin 14 (ab7800 Abcam), rabbit DPM1 (#12403-2-AP, Proteintech), rabbit SERPINB5 (MASPIN #ab182785 Abcam), rabbit pSMAD1/3/5 (#ab95455 Abcam), rabbit pSMAD2/3 (#AP0548 Lubioscience, Zürich, Switzerland), mouse SMAD2/3 (#sc-133098 Santa Cruz), rabbit mGFP (#TA150122 Thermo Fisher Scientific), mouse GAPDH mAb (clone 0411, #sc-47724 Santa Cruz), mouse α tubulin (clone 10D8, #627901 BioLegend). Goat anti-mouse 800CW and goat anti-rabbit 680RD (#925-32210 and #925-68071, both Li-Cor) were used as secondary antibodies, incubated for 1 h at room temperature. Odyssey FC imaging system was used for imaging the blots and band density was quantified with Image Studio (both Li-Cor).

Immunoprecipitation

Confluent cell monolayers were washed twice with ice-cold PBS and incubated with modified RIPA buffer plus protease inhibitors (10 mM Na_2HPO_4, 150 mM NaCl, 1%Triton X-100, 0.25% SDS, 1% sodium deoxycholate, pH 7.3), for 30 min on ice. Cells were then scraped and homogenized on ice by passing 10 times through a 20G and 25G injection needle. Cell debris were removed by centrifugation at 7000g, 5 min, 4°C. Protein concentration was determined by BCA (Thermo Fisher Scientific) and equal amounts of protein were diluted in 1ml of RIPA buffer. GFP trap magnetic agarose beads (gtma-20 ChromoTek, Martinsried, Germany) were washed 3 times (3X) with 1ml RIPA buffer and 25µl of beads were added to diluted lysates and incubated for 1.5 hrs at 4°C. Beads were washed twelve times with wash buffers and afterwards mixed with Laemmli buffer and denaturized at 95°C for 10 min. The following samples from I.P were subjected to western blotting as described above. Rabbit mGFP (#TA150122 Thermo Fisher Scientific) primary antibody was used to confirm immunoprecipitation and mouse DSP mAb (#sc-390975 Santa Cruz) antibody was used to detect desmoplakin co-immunoprecipitation.

Dispase - based dissociation assay

HaCaT keratinocytes expressing various sgRNA and overexpression constructs or primary human keratinocytes were seeded in equal numbers in 24-well plates. After reaching confluency, cells were washed with pre-warmed PBS and incubated with 250 µl dispase II (50mg/10ml in HBSS; Sigma-Aldrich D4693) for 20 min (HaCaTs) and 45 min for primary human keratinocytes at 37°C to detach the intact cell sheet from the well bottom. 150ul HBSS was added to these wells and a constant mechanical shear stress was applied using an electrical pipette (Eppendorf, Hamburg, Germany), for 10 times each well. Wells were finally imaged with a binocular microscope (Olympus, Tokyo, Japan) and SLR camera (Canon, Tokyo, Japan). The number of fragments generated are a direct measure cell cohesion, which is inversely proportional to adhesive strength.

Immunostaining

Cells were grown on 13 mm glass coverslips and fixed with either 2% PFA (Thermo Fisher Scientific) in PBS at room temperature or ice-cold methanol (Merck Millipore) for 10 min on ice.

Cells were permeabilized with 0.1% Triton X-100 in PBS for 10 min and blocked with 3% BSA and 1% normal goat serum in PBS for 1 h, in a humidified chamber. The following primary antibodies were incubated overnight at 4°C: mouse Dsg2 mAb (clone 10G11, #BM5016 Acris), rabbit Dsg2 pAb (#610121 Progen), mouse Dsg3 mAb (clone 5G11, # 326300 Invitrogen, Carlsbad, CA, USA), rabbit DSP pAb (NW39), mouse DSP mAb (1G4) (both kind gifts from Kathleen Green, Northwestern University, Chicago, USA), Phalloidin CruzFluor 488 (#sc-363791 Santa Cruz), pan-cytokeratin (AE1/AE3) efluor 570 (#41-9003-80 eBioscience). Following primary antibody incubation, cells were washed 3 times with PBS and AlexaFluor (AF488, AF568) conjugated anti-rabbit or anti-mouse antibodies (#A-11008, A-11004 Fisher Scientific) were added and incubated for 1 h at room temperature. DAPI (Sigma-Aldrich) was added for 10 min to counterstain nuclei. Cells were washed 3 times with PBS and mounted with ProLong Diamond Antifade (Thermo Fisher Scientific). Image acquisitions were done using Stellaris 8 Falcon confocal microscope (Leica, Wetzlar, Germany) with a HC PL APO CS2 63x/1.40 oil objective. Image analysis was done with ImageJ software for analyzing plot profiles and counting DSP puncta as described later in data analysis section.

For staining of paraffin sections, tissues embedded in paraffin were cut into 5 µm thick sections with an automated microtome (HM355S, Thermo Fisher Scientific). After deparaffinization, temperature-mediated antigen retrieval was performed in citrate buffer (10 mM citric acid monohydrate (VWR, 20276.235, Pennsylvania, USA), pH6, 0.1 % triton X-100) for 20 min at 95 °C. Tissue was permeabilized in 0.1 % triton X-100 in PBS for 5 min and blocked with 3 % bovine serum albumin/0.12 % normal goat serum in PBS for 1 hour. The following primary antibodies were incubated in PBS at 4 °C overnight: mouse DSP (#61003 Progen), rabbit DSG2 RB5 (# 610120 Progen Biotechnik), rabbit pSMAD2(S465/S467)/pSMAD3(S423/S425) (#AP0548 Lubioscience), rabbit pSMAD1/3/5(#ab95455 Abcam), Filaggrin (#ab218395 Abcam), Keratin 10 (#905403 Biolegend), Ki67 B56 (#550609 BD Bioscience), rabbit SERPINB5 (MASPIN #ab182785 Abcam), rabbit DPM1 (#12403-2-AP, Proteintech). Respective secondary goat anti-rabbit or goat anti-mouse antibodies coupled to Alexa Fluor 488, Alexa Fluor 568 (both Thermo Fisher Scientific), or cy5 (Dianova, Hamburg, Germany) were incubated for 1 hour at room temperature and DAPI (Sigma-Aldrich) was added for 10 min to counterstain nuclei. Finally, samples were mounted with Fluoromount Aqueous Mounting Medium (Sigma-Aldrich).

Histology:

Fixed 3D-RHEs were cut from the cell culture insert using a 8 mm biopsy punch (#600213 Stiefel), cut into half and embedded in histogel (#HG-4000-012 Epredia). After polymerization of the histogel, samples were stored in PBS at 4°C until paraffin embedding using the TPC 15 Tissue Processor (Medite Medizintechnik): 1) 70% ethanol, 37°C, 45 min; 2) 80% ethanol, 37°C, 45 min; 3) 96% ethanol, 37°C, 30 min; 4) 96% ethanol, 37°C, 45 min; 5) 100% ethanol, 37°C, 30 min; 6) 100% ethanol, 37°C, 60 min; 7) 100% ethanol, 37°C, 60 min; 8) Xylene, 37°C, 30 min; 9) Xylene, 37°C, 45 min; 10) Xylene, 37°C, 60 min; 11) Paraffin, 62°C, 45 min; 12) Paraffin, 62°C, 60 min; 13) Paraffin, 62°C, 60 min.TES Valida embedding station (Medite Medizintechnik) was used to embed processed tissue into paraffin blocks and cut into 5 µm sections using an automated microtome (HM355S, Thermo Fisher Scientific). Haematoxylin and Eosin (H&E) staining was performed according to standard procedures. In brief, sections were stained with mayer's haemalaun solution (#1.09249.1022 Sigma-Aldrich) for 5 min, washed, dehydrated in an increasing ethanol series and stained with 0.5 % (w/v) eosin solution for 5 min. After washing steps

in ethanol and methyl salicylate, sections were mounted with DPX mounting media (#06522 Sigma-Aldrich).

Atomic Force Microscopy (AFM)

A Nanowizard IV atomic force microscope (AFM, JPK Instruments, Berlin, Germany) mounted on an inverted fluorescence microscope (IX83, Olympus) was used for cell stiffness measurements. Experiments were performed in culture medium at 37°C using Si3N4 AFM cantilevers (pyramid-shaped D-tip, MLCT cantilever, Bruker, 4 Billerica, MA, USA) with a spring constant of 0.03 N/m. Spring constant was calibrated for each cantilever at 37 °C applying the thermal noise method. Force-displacement curves were obtained in force spectroscopy mode using the following settings: relative setpoint 0.4 nN, z-length 5 µm, extend delay 0 s, pulling speed 2 µm/s, and recorded with the SPM control v.4 software 15 (JPK Instruments). Cells were seeded on glass coverslips. All measurements were performed in the cell center and conducted within 1 h. Force distance curves were analyzed using JPKSPM Data Processing software (version 6, JPK Instruments) and then fitted with the Hertz model for young's modulus calculation. The tip-half opening angle was 17.5 degrees, the poisson ratio was set as 0.5 and 300 nm of indentation depth was used.

Fluorescence Recovery After Photobleaching (FRAP)

For FRAP measurements, HaCaT cells (sgNT1) and sgDPM1 were transduced with DSP-GFP[28] as described above and seeded in 8-well imaging chambers (IBIDI). After the formation of visible junctions, FRAP measurements were performed on a Stellaris 8 Falcon confocal microscope (Leica) with a HC PL APO CS2 63x/1.40 oil objective, at 37 °C with 5 % CO2 and constant humidity. The measurements were carried out and analyzed with the fluorescence recovery after photobleaching wizard software (Leica). Regions of interests were defined along cell-cell junctions containing a desmosome between two neighboring mGFP positive cells. After 5 frames of recording the prebleach intensity, mGFP signal was bleached shortly for 5 frames, using the 488 nm laser line at 80 % transmission on FRAP booster mode and the fluorescence recovery was recorded over 239 s with 100 frames for the initial 26 s and 45 frames for the remaining time. The fraction of mobile molecules was determined by the formula: Mobile fraction = Ie – Io/ Ii – Io, where, Ie is the intensity reached after recovery time, Io is the minimal intensity that was achieved right after bleaching, and Ii is the average prebleach intensity value.

Proteomics

<u>Sample preparation for enrichment analysis:</u>

Samples were adjusted to the 5% of SDS, 100 mM TEAB and 10 mM TCEP and subsequently reduced for 10 min at 95°C. Samples were then cooled down to RT and 0.5 µL of 1M iodoacetamide was added to the samples. Cysteine residues were alkylated for 30 min at 25°C in the dark. Digestion and peptide purification were performed using S-trap technology (Protifi) according to the manufacturer's instructions. In brief, samples were acidified by addition of 2.5 µL of 12% phosphoric acid (1:10) and then 165 µL of S-trap buffer (90% methanol, 100 mM TEAB pH 7.1) was added to the samples (6:1). Samples were briefly vortexed and loaded onto S-trap micro spin-columns (Protifi) and centrifuged for 1 min at 4000 g. Flow-through was discarded and spin-columns were then washed 3 times with 150 µL of S-trap buffer (each time samples were centrifuged for 1 min at 4000 g and flow-through was removed). S-trap columns were then moved to the clean tubes and 20 µL of digestion buffer (50 mM TEAB pH 8.0) and trypsin (at 1:25 enzyme to protein ratio) were added to the samples. Digestion was allowed to proceed for 1h at 47 °C.

After, 40 µL of digestion buffer was added to the samples and the peptides were collected by centrifugation at 4000 g for 1 minute. To increase the recovery, S-trap columns were washed with 40 µL of 0.2% formic acid in water (400g, 1 min) and 35 µL of 0.2% formic acid in 50% acetonitrile. Eluted peptides were dried under vacuum and stored at -20 ℃ until further analysis.

Data acquisition for enrichment analysis:

Dried peptides were resuspended 0.1% FA and 0.2 ug of peptides were subjected to LC–MS/MS analysis using a Q Exactive Plus Mass Spectrometer fitted with an EASY-nLC 1000 (both Thermo Fisher Scientific) and a custom-made column heater set to 60°C. Peptides were resolved using a RP-HPLC column (75µm × 30cm) packed in-house with C18 resin (ReproSil-Pur C18–AQ, 1.9 µm resin; Dr. Maisch GmbH) at a flow rate of 0.2 µLmin-1. A linear gradient ranging from 5% buffer B to 45% buffer B over 60 min was used for peptide separation. Buffer A was 0.1% formic acid in water and buffer B was 80% acetonitrile, 0.1% formic acid in water. The mass spectrometer was operated in DDA mode with a total cycle time of approximately 1 s. Each MS1 scan was followed by high-collision-dissociation (HCD) of the 20 most abundant precursor ions with dynamic exclusion set to 5 s. For MS1, 3e6 ions were accumulated in the Orbitrap over a maximum time of 25 ms and scanned at a resolution of 70,000 FWHM (at 200 m/z). MS2 scans were acquired at a target setting of 1e5 ions, maximum accumulation time of 110 ms and a resolution of 35,000 FWHM (at 200 m/z). Singly charged ions, ions with charge state ≥ 6 and ions with unassigned charge state were excluded from triggering MS2 events. The normalized collision energy was set to 27%, the mass isolation window was set to 1.4 m/z and one microscan was acquired for each spectrum.

Sample preparation for total proteomics:

Cells were lysed in 50 µL of lysis buffer (1% Sodium deoxycholate (SDC), 10 mM TCEP, 100 mM Tris, pH=8.5) using twenty cycles of sonication (30s on, 30 s off per cycle) on a Bioruptor (Dianode). Following sonication, proteins in the bacterial lysate were reduced by TCEP at 95° C for 10 min. Proteins were alkylated using 15 mM chloroacetamide at 37° C for 30 min and further digested using sequencing-grade modified trypsin (1/50 w/w, ratio trypsin/protein; Promega, USA) at 37° C for 12 h. After digestion, the samples were acidified using TFA (final 1%). Peptide desalting was performed using iST cartridges (PreOmics, Germany) following the manufactures instructions. After drying the samples under vacuum, peptides were stored at -20° C and dissolved in 0.1% aqueous formic acid solution at a concentration of 0.5 mg/ml upon use.

Data acquisition for total proteomics:

Dried peptides were resuspended 0.1% FA and 0.2 ug of peptides were subjected to LC–MS/MS analysis using a Orbitrap Fusion Lumos Mass Spectrometer fitted with an EASY-nLC 1200 (both Thermo Fisher Scientific) and a custom-made column heater set to 60°C. Peptides were resolved using a RP-HPLC column (75µm × 36cm) packed in-house with C18 resin (ReproSil-Pur C18–AQ, 1.9 µm resin; Dr. Maisch GmbH) at a flow rate of 0.2 µLmin-1. The following gradient was used for peptide separation: from 5% B to 12% B over 5 min to 35% B over 65 min to 50% B over 20 min to 95% B over 2 min followed by 18 min at 95% B. Buffer A was 0.1% formic acid in water and buffer B was 80% acetonitrile, 0.1% formic acid in water. The mass spectrometer was operated in DDA mode with a cycle time of 3 s between master scans. Each master scan was acquired in the Orbitrap at a resolution of 120,000 FWHM (at 200 m/z) and a scan range from 375 to 1500 m/z followed by MS2 scans of the most intense precursors in the linear ion trap at “Rapid”

scan rate with isolation width of the quadrupole set to 1.4 m/z. Maximum ion injection time was set to 50ms (MS1) and 35 ms (MS2) with an AGC target set to 1e6 and 1e4, respectively. Only peptides with charge state 2 – 5 were included in the analysis. Monoisotopic precursor selection (MIPS) was set to Peptide, and the Intensity Threshold was set to 5e3. Peptides were fragmented by HCD (Higher-energy collisional dissociation) with collision energy set to 35%, and one microscan was acquired for each spectrum. The dynamic exclusion duration was set to 30s.

Image Processing and Statistics

Figures were compiled with Photoshop CC and Illustrator CC (Adobe, San José, CA, USA). Statistical analysis was performed using GraphPad Prism 8 with a two-tailed student's t-test for the comparison of two data sets and one-way or two-way ANOVA corrected by either Dunnett's, Dunn's or Tukey's test for more than two data sets. Statistical significance was determined at $p < 0.05$. The data sets were first tested for normal distribution using Shapiro-Wilk normality test and respective statistics were applied based on the distribution. Welch correction for unequal variances was applied where applicable. The error bars shown in all graphs were depicted as ± SD. A minimum of 3 biological replicates was used in each experiment.

Data Analysis:

- **Epidermal thickness analysis:**
  Epidermal thickness was analyzed on H&E-stained tissue sections by using the image analysis software QuPath[62]. In brief, 3-5 images per section were analyzed in QuPath by marking a rectangular area of the tissue section and then applying the "wand" tool to mark the different layers of the epidermis. The area of these were measured and divided by the total length of the epidermis. The following formula was applied to calculate the tissue thickness.

$$\frac{Tissue\ area\ [\mu m^2]}{Tissue\ length\ [\mu m]} = tissue\ thickness\ [\mu m]$$

  Corneal layer and non-corneal layer (viable) thickness were normalized to total epidermal thickness, to account for variances in overall thickness across biological replicates.
- **Ki67 analysis of 3D-RHE:**
  Proliferation of 3D-RHE was analyzed on Ki67 staining from tissue sections, using QuPath software [62]. In brief, 3-5 images per sample were analyzed in QuPath and nuclei were masked by detecting DAPI signal. The total numbers of nuclei per field were quantified. From these masks generated, Ki67 positive nuclei were counted and the ratio of Ki67 positive nuclei to total nuclei was calculated to determine the percentage of Ki67 positive cells.
- **ImageJ Analysis:**
  Image J was used to generate kymographs of FRAP recovery data for DSP GFP signal over dynamic time scales before and after bleaching.
  Keratin distribution and cortical actin distribution were analyzed by drawing a ROI rectangle of fixed size at the cell-cell contact sites (10 micron) and measuring the mean plot

profile intensities along this area for individual cells. GraphPad PRISM software was used to create graphs and statistical analysis.

DSP dots were quantified by applying a threshold to the DSP staining on images, such that all the DSP puncta were accounted for. The membrane length for individual cells was measured by drawing ROI around the cell membranes and the respective number of DSP puncta over this cell were counted using particle analysis in ImageJ.

- **Proteomic data analysis:**

  The raw were analyzed using MaxQuant (v1.6.17.0)[63] with default setting. In brief, the spectra were searched against a human database (protein sequences downloaded from www.uniprot.org on 2020/04/17) and commonly observed contaminants by the Andromeda search engine [64], using the following search criteria: full tryptic specificity was required (cleavage after lysine or arginine residues, unless followed by proline); 3 missed cleavages were allowed; carbamidomethylation (C) was set as fixed modification; oxidation (M) and acetylation (Protein N-term) were applied as variable modifications; mass tolerance of 20 ppm (precursor) and 20 ppm/0.6 Da (fragments) for QE-plus/Lumos. Label-free and iBAQ quantification as well as much between runs were enabled. The database search results were filtered to a false discovery rate (FDR) to 1% on the peptide and protein level and specified a minimum length of 7 amino acids for peptides. Quantitative analysis results from label-free quantification were processed using the MSstats R package v4.0.1[65].

  Heat maps were generated by using ClustVis software freely available as an online tool. STRING database was used to identify molecular and biological pathways associated with the significantly modulated proteins across the samples.

ACKNOWLEDGEMENTS:

The authors would like to acknowledge Dr. Diego Calabrese (Histology Core Facility); and Drs. Mike Abanto and Pascal Lorentz (Microscopy Core Facility), University of Basel, Switzerland, Dr. Katarzyna Buczak, Proteomics Facility Basel (Biocentre, University of Basel), Prof. Kathleen Green, Northwestern University, USA) for providing desmoplakin antibodies and Addgene plasmid #32227, Department of Urology (University hospital, Basel) for providing human foreskin tissues, Swiss National Science Foundation- SNSF (#197764 to Dr. Spindler) for funding.

DISCLOSURES:

The authors declare no conflict of interest.

REFERENCES:

1. Broussard, J.A., S. Getsios, and K.J. Green, *Desmosome regulation and signaling in disease.* Cell Tissue Res, 2015. **360**(3): p. 501-12.
2. Najor, N.A., *Desmosomes in Human Disease.* Annu Rev Pathol, 2018. **13**: p. 51-70.
3. Yang, Z., et al., *Desmosomal dysfunction due to mutations in desmoplakin causes arrhythmogenic right ventricular dysplasia/cardiomyopathy.* Circ Res, 2006. **99**(6): p. 646-55.
4. Delva, E., D.K. Tucker, and A.P. Kowalczyk, *The desmosome.* Cold Spring Harb Perspect Biol, 2009. **1**(2): p. a002543.
5. Chitaev, N.A. and S.M. Troyanovsky, *Direct Ca2+-dependent heterophilic interaction between desmosomal cadherins, desmoglein and desmocollin, contributes to cell-cell adhesion.* J Cell Biol, 1997. **138**(1): p. 193-201.
6. Nie, Z., et al., *Membrane-impermeable cross-linking provides evidence for homophilic, isoform-specific binding of desmosomal cadherins in epithelial cells.* J Biol Chem, 2011. **286**(3): p. 2143-54.
7. Harrison, O.J., et al., *Structural basis of adhesive binding by desmocollins and desmogleins.* Proc Natl Acad Sci U S A, 2016. **113**(26): p. 7160-5.
8. Kouklis, P.D., E. Hutton, and E. Fuchs, *Making a connection: direct binding between keratin intermediate filaments and desmosomal proteins.* J Cell Biol, 1994. **127**(4): p. 1049-60.
9. Godsel, L.M., et al., *Desmoplakin assembly dynamics in four dimensions: multiple phases differentially regulated by intermediate filaments and actin.* J Cell Biol, 2005. **171**(6): p. 1045-59.
10. Candi, E., R. Schmidt, and G. Melino, *The cornified envelope: a model of cell death in the skin.* Nat Rev Mol Cell Biol, 2005. **6**(4): p. 328-40.
11. Jonkman, M.F., et al., *Loss of desmoplakin tail causes lethal acantholytic epidermolysis bullosa.* Am J Hum Genet, 2005. **77**(4): p. 653-60.
12. Chidgey, M., et al., *Mice lacking desmocollin 1 show epidermal fragility accompanied by barrier defects and abnormal differentiation.* J Cell Biol, 2001. **155**(5): p. 821-32.
13. Sumigray, K.D. and T. Lechler, *Cell adhesion in epidermal development and barrier formation.* Curr Top Dev Biol, 2015. **112**: p. 383-414.
14. Koch, P.J., et al., *Targeted disruption of the pemphigus vulgaris antigen (desmoglein 3) gene in mice causes loss of keratinocyte cell adhesion with a phenotype similar to pemphigus vulgaris.* J Cell Biol, 1997. **137**(5): p. 1091-102.
15. Spindler, V. and J. Waschke, *Pemphigus-A Disease of Desmosome Dysfunction Caused by Multiple Mechanisms.* Front Immunol, 2018. **9**: p. 136.
16. Ruoslahti, E., *Proteoglycans in cell regulation.* J Biol Chem, 1989. **264**(23): p. 13369-72.
17. Ruoslahti, E. and Y. Yamaguchi, *Proteoglycans as modulators of growth factor activities.* Cell, 1991. **64**(5): p. 867-9.
18. Stanley, P., et al., *Essentials of glycobiology.* Varki, A, 2009.
19. Maeda, Y., et al., *DPM2 regulates biosynthesis of dolichol phosphate-mannose in mammalian cells: correct subcellular localization and stabilization of DPM1, and binding of dolichol phosphate.* EMBO J, 1998. **17**(17): p. 4920-9.
20. Kornfeld, R. and S. Kornfeld, *Assembly of asparagine-linked oligosaccharides.* Annu Rev Biochem, 1985. **54**: p. 631-64.
21. Herscovics, A. and P. Orlean, *Glycoprotein biosynthesis in yeast.* FASEB J, 1993. **7**(6): p. 540-50.
22. Kim, S., et al., *Dolichol phosphate mannose synthase (DPM1) mutations define congenital disorder of glycosylation Ie (CDG-Ie).* J Clin Invest, 2000. **105**(2): p. 191-8.
23. Jin, S.P. and J.H. Chung, *Inhibition of N-glycosylation by tunicamycin attenuates cell-cell adhesion via impaired desmosome formation in normal human epidermal keratinocytes.* Biosci Rep, 2018. **38**(6).

24. Brodehl, A., et al., *Incorporation of desmocollin-2 into the plasma membrane requires N-glycosylation at multiple sites.* FEBS Open Bio, 2019. **9**(5): p. 996-1007.
25. Hatsell, S., et al., *Plakoglobin is O-glycosylated close to the N-terminal destruction box.* J Biol Chem, 2003. **278**(39): p. 37745-52.
26. Dabelsteen, S., et al., *Essential Functions of Glycans in Human Epithelia Dissected by a CRISPR-Cas9-Engineered Human Organotypic Skin Model.* Dev Cell, 2020. **54**(5): p. 669-684 e7.
27. Walsh, A. and S.J. Chapman, *Sugars protect desmosome and corneosome glycoproteins from proteolysis.* Arch Dermatol Res, 1991. **283**(3): p. 174-9.
28. Wanuske, M.T., et al., *Clustering of desmosomal cadherins by desmoplakin is essential for cell-cell adhesion.* Acta Physiol (Oxf), 2021. **231**(4): p. e13609.
29. Ramms, L., et al., *Keratins as the main component for the mechanical integrity of keratinocytes.* Proc Natl Acad Sci U S A, 2013. **110**(46): p. 18513-8.
30. Asrani, K., et al., *mTORC1 loss impairs epidermal adhesion via TGF-beta/Rho kinase activation.* J Clin Invest, 2017. **127**(11): p. 4001-4017.
31. Wang, S.E., et al., *Convergence of p53 and transforming growth factor beta (TGFbeta) signaling on activating expression of the tumor suppressor gene maspin in mammary epithelial cells.* J Biol Chem, 2007. **282**(8): p. 5661-9.
32. Bizet, A.A., et al., *The TGF-beta co-receptor, CD109, promotes internalization and degradation of TGF-beta receptors.* Biochim Biophys Acta, 2011. **1813**(5): p. 742-53.
33. Kljuic, A., et al., *Desmoglein 4 in hair follicle differentiation and epidermal adhesion: evidence from inherited hypotrichosis and acquired pemphigus vulgaris.* Cell, 2003. **113**(2): p. 249-60.
34. Getsios, S., et al., *Desmoglein 1-dependent suppression of EGFR signaling promotes epidermal differentiation and morphogenesis.* J Cell Biol, 2009. **185**(7): p. 1243-58.
35. Elias, P.M., et al., *Desmoglein isoform distribution affects stratum corneum structure and function.* J Cell Biol, 2001. **153**(2): p. 243-9.
36. Merritt, A.J., et al., *Suprabasal desmoglein 3 expression in the epidermis of transgenic mice results in hyperproliferation and abnormal differentiation.* Mol Cell Biol, 2002. **22**(16): p. 5846-58.
37. Allen, E., Q.C. Yu, and E. Fuchs, *Mice expressing a mutant desmosomal cadherin exhibit abnormalities in desmosomes, proliferation, and epidermal differentiation.* J Cell Biol, 1996. **133**(6): p. 1367-82.
38. Runswick, S.K., et al., *Desmosomal adhesion regulates epithelial morphogenesis and cell positioning.* Nat Cell Biol, 2001. **3**(9): p. 823-30.
39. Dehner, C., et al., *A desmoplakin point mutation with enhanced keratin association ameliorates pemphigus vulgaris autoantibody-mediated loss of cell cohesion.* Am J Pathol, 2014. **184**(9): p. 2528-36.
40. Spindler, V., et al., *Mechanisms Causing Loss of Keratinocyte Cohesion in Pemphigus.* J Invest Dermatol, 2018. **138**(1): p. 32-37.
41. Vielmuth, F., et al., *Keratins Regulate the Adhesive Properties of Desmosomal Cadherins through Signaling.* J Invest Dermatol, 2018. **138**(1): p. 121-131.
42. Kroger, C., et al., *Keratins control intercellular adhesion involving PKC-alpha-mediated desmoplakin phosphorylation.* J Cell Biol, 2013. **201**(5): p. 681-92.
43. Loranger, A., et al., *Keratin 8 modulation of desmoplakin deposition at desmosomes in hepatocytes.* Exp Cell Res, 2006. **312**(20): p. 4108-19.
44. Loschke, F., M. Homberg, and T.M. Magin, *Keratin Isotypes Control Desmosome Stability and Dynamics through PKCalpha.* J Invest Dermatol, 2016. **136**(1): p. 202-13.
45. Rotzer, V., et al., *Adducin is required for desmosomal cohesion in keratinocytes.* J Biol Chem, 2014. **289**(21): p. 14925-40.
46. Hiermaier, M., et al., *The Actin-Binding Protein alpha-Adducin Modulates Desmosomal Turnover and Plasticity.* J Invest Dermatol, 2021. **141**(5): p. 1219-1229 e11.

47. Godsel, L.M., et al., *Plakophilin 2 couples actomyosin remodeling to desmosomal plaque assembly via RhoA.* Mol Biol Cell, 2010. **21**(16): p. 2844-59.
48. Todorovic, V., et al., *Plakoglobin regulates cell motility through Rho- and fibronectin-dependent Src signaling.* J Cell Sci, 2010. **123**(Pt 20): p. 3576-86.
49. Akiyama, M., *Corneocyte lipid envelope (CLE), the key structure for skin barrier function and ichthyosis pathogenesis.* J Dermatol Sci, 2017. **88**(1): p. 3-9.
50. Feingold, K.R., *The outer frontier: the importance of lipid metabolism in the skin.* J Lipid Res, 2009. **50 Suppl**(Suppl): p. S417-22.
51. Vietri Rudan, M., et al., *Human epidermal stem cell differentiation is modulated by specific lipid subspecies.* Proc Natl Acad Sci U S A, 2020. **117**(36): p. 22173-22182.
52. Pemberton, P.A., et al., *The tumor suppressor maspin does not undergo the stressed to relaxed transition or inhibit trypsin-like serine proteases. Evidence that maspin is not a protease inhibitory serpin.* J Biol Chem, 1995. **270**(26): p. 15832-7.
53. Maass, N., et al., *Down regulation of the tumor suppressor gene maspin in breast carcinoma is associated with a higher risk of distant metastasis.* Clin Biochem, 2001. **34**(4): p. 303-7.
54. Jiang, N., et al., *Maspin sensitizes breast carcinoma cells to induced apoptosis.* Oncogene, 2002. **21**(26): p. 4089-98.
55. Gao, F., et al., *Maspin plays an essential role in early embryonic development.* Development, 2004. **131**(7): p. 1479-89.
56. Qin, L. and M. Zhang, *Maspin regulates endothelial cell adhesion and migration through an integrin signaling pathway.* J Biol Chem, 2010. **285**(42): p. 32360-9.
57. Tamazato Longhi, M., et al., *EGFR Signaling Regulates Maspin/SerpinB5 Phosphorylation and Nuclear Localization in Mammary Epithelial Cells.* PLoS One, 2016. **11**(7): p. e0159856.
58. Badu-Nkansah, K.A. and T. Lechler, *Proteomic analysis of desmosomes reveals novel components required for epidermal integrity.* Mol Biol Cell, 2020. **31**(11): p. 1140-1153.
59. Sellheyer, K., et al., *Inhibition of skin development by overexpression of transforming growth factor beta 1 in the epidermis of transgenic mice.* Proc Natl Acad Sci U S A, 1993. **90**(11): p. 5237-41.
60. Zheng, H., et al., *SerpinB7 deficiency contributes to development of psoriasis via calcium-mediated keratinocyte differentiation dysfunction.* Cell Death Dis, 2022. **13**(7): p. 635.
61. Boukamp, P., et al., *Normal keratinization in a spontaneously immortalized aneuploid human keratinocyte cell line.* J Cell Biol, 1988. **106**(3): p. 761-71.
62. Bankhead, P., et al., *QuPath: Open source software for digital pathology image analysis.* Scientific Reports, 2017. **7**(1): p. 16878.
63. Cox, J. and M. Mann, *MaxQuant enables high peptide identification rates, individualized p.p.b.-range mass accuracies and proteome-wide protein quantification.* Nat Biotechnol, 2008. **26**(12): p. 1367-72.
64. Cox, J., et al., *Andromeda: a peptide search engine integrated into the MaxQuant environment.* J Proteome Res, 2011. **10**(4): p. 1794-805.
65. Choi, M., et al., *MSstats: an R package for statistical analysis of quantitative mass spectrometry-based proteomic experiments.* Bioinformatics, 2014. **30**(17): p. 2524-6.

Figure 1

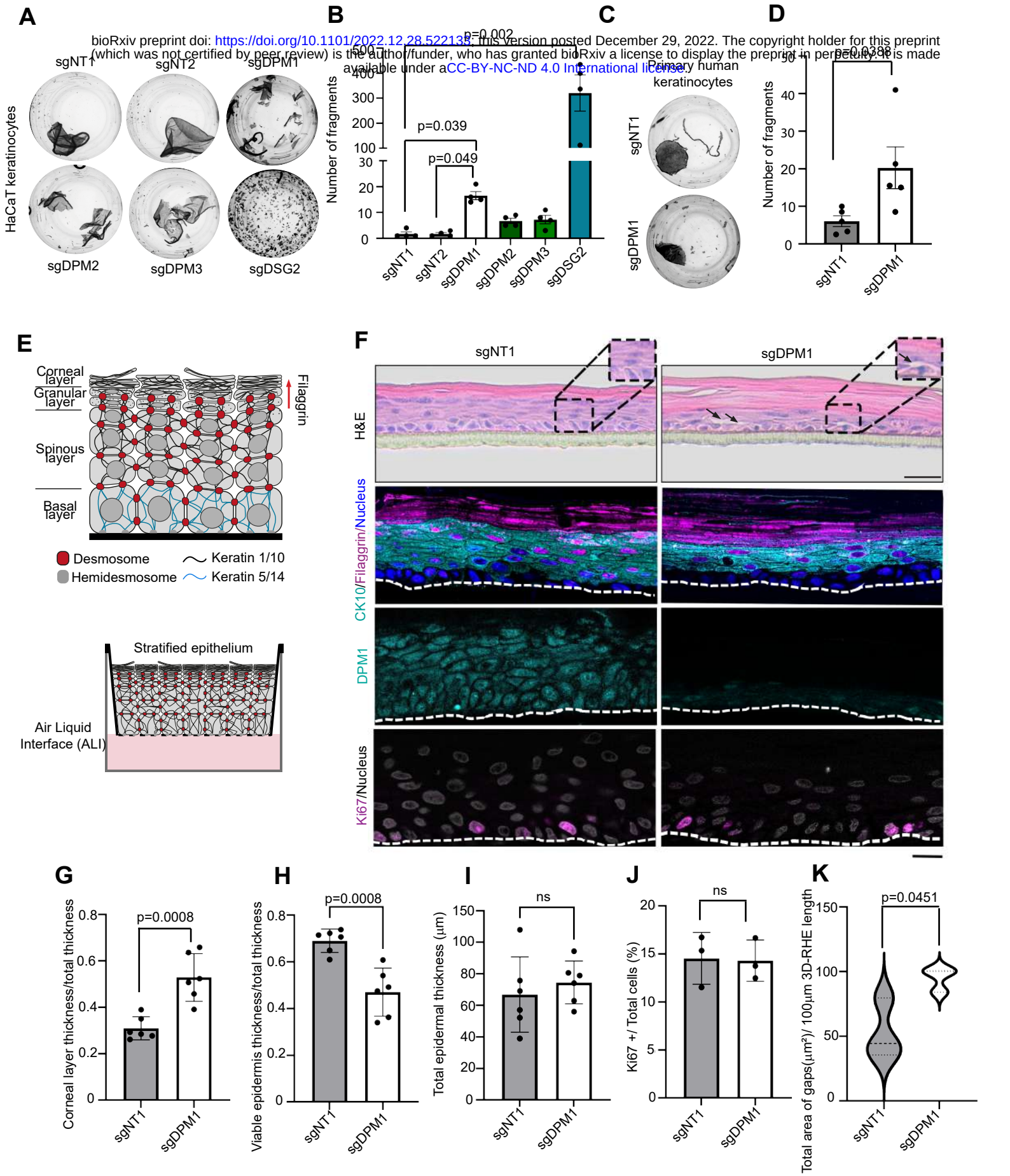

Figure 2

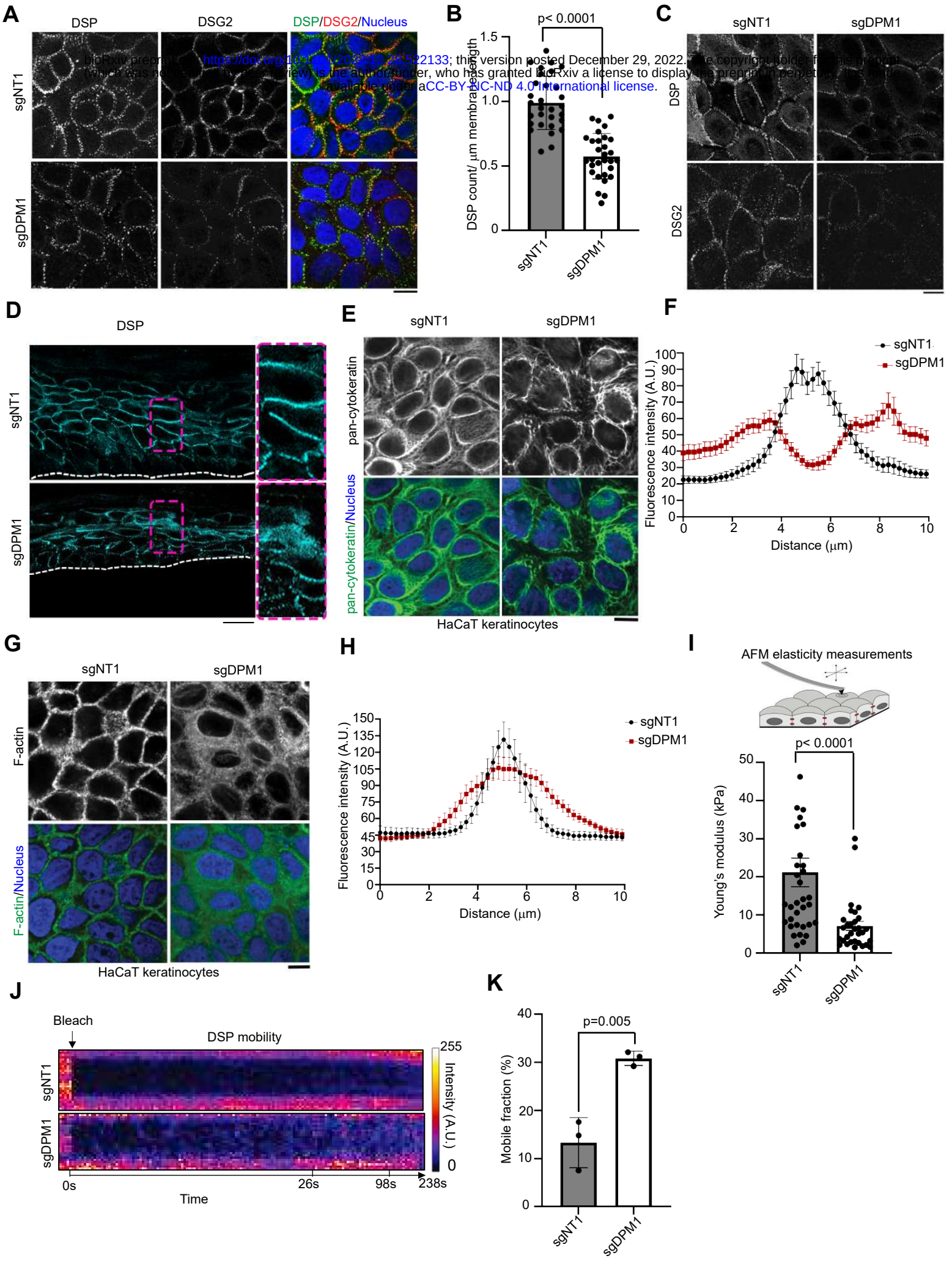

Figure 3

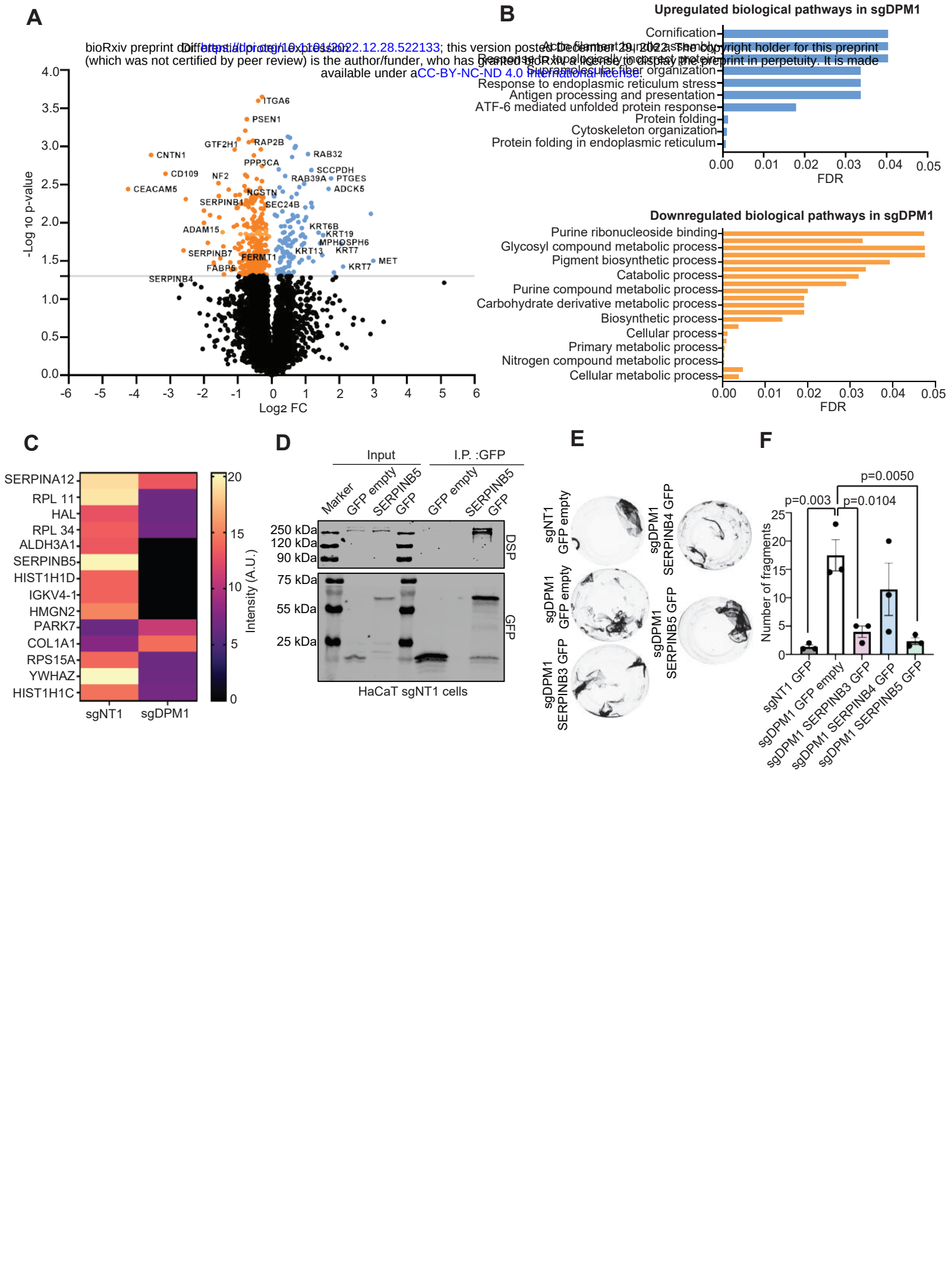

Figure 4

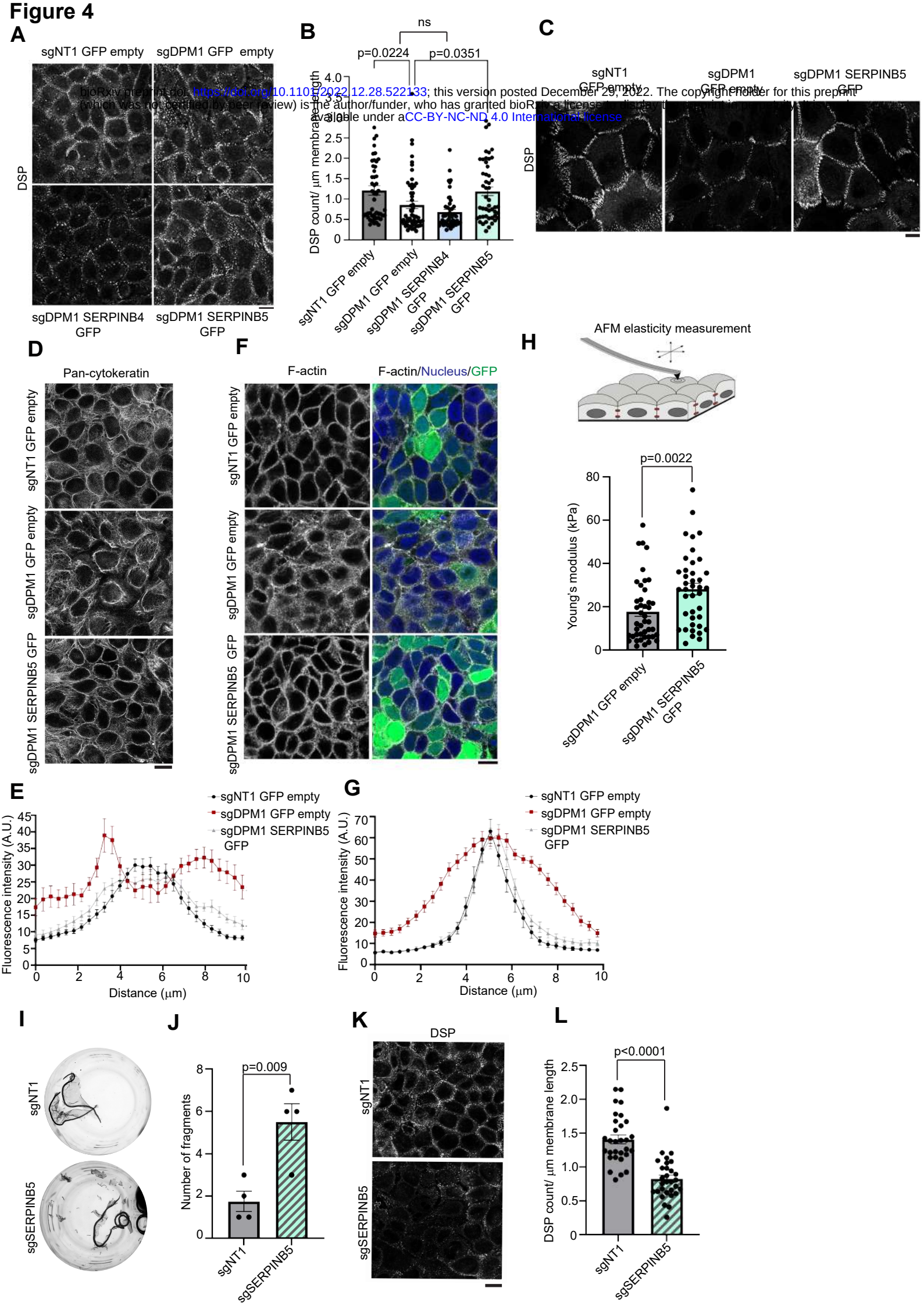

Figure 5

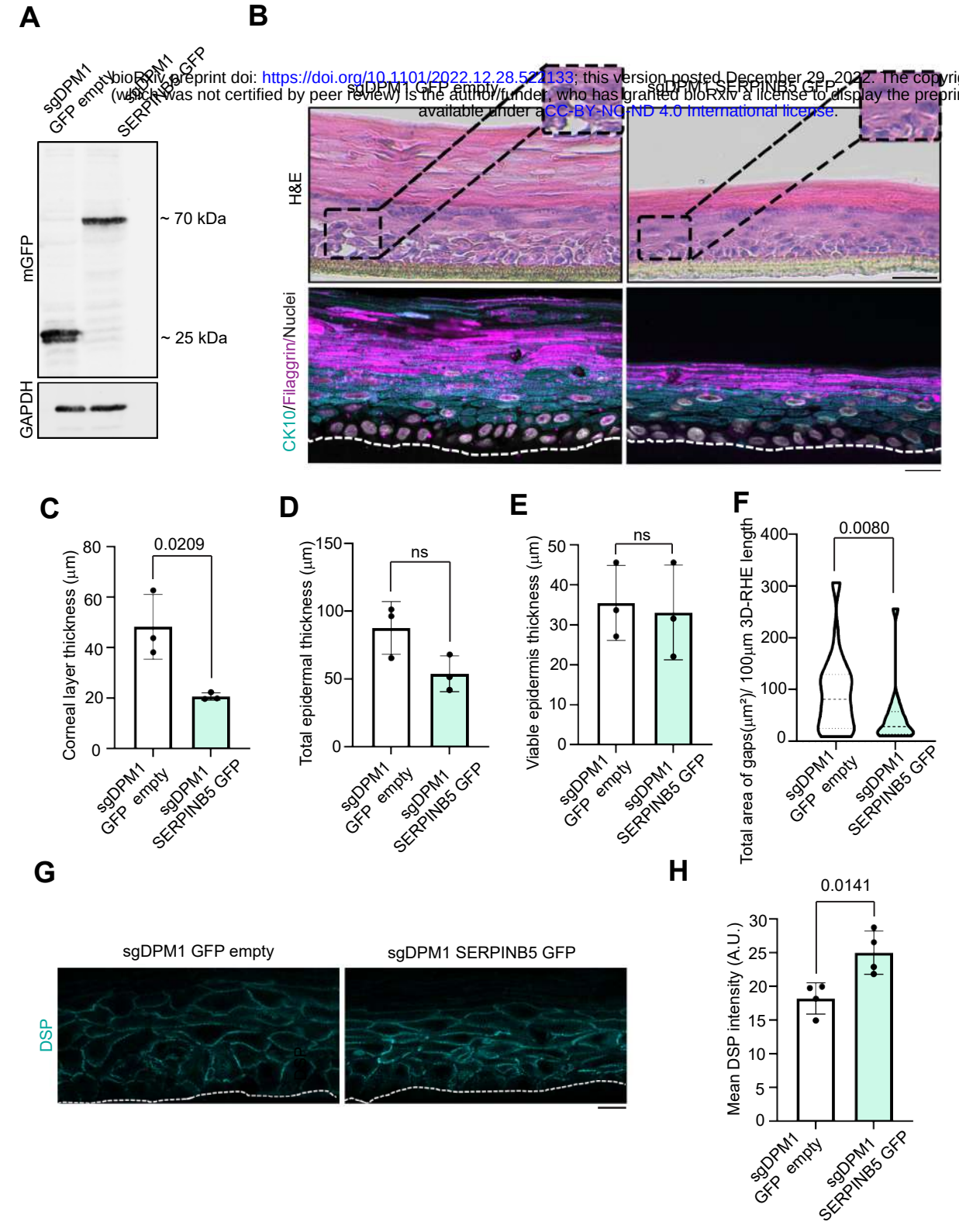

Figure 6